Veterinary Microbiology 230 (2019) 283–290

Contents lists available at ScienceDirect

Veterinary Microbiology

journal homepage: www.elsevier.com/locate/vetmic

Syncytia generated by hemagglutinin-neuraminidase and fusion proteins of virulent Newcastle disease virus induce complete autophagy by activating AMPK-mTORC1-ULK1 signaling >

Shanhui Ren[a], Zaib Ur Rehman[a], Mengyu Shi[a], Bin Yang[b], Yurong Qu[a], Xiao Feng Yang[a], Qi Shao[a], Chunchun Meng[a], Zengqi Yang[c], Xiaolong Gao[d], Yingjie Sun[a,*], Chan Ding[a,e,*]

[a] Department of Avian Infectious Diseases, Shanghai Veterinary Research Institute, Chinese Academy of Agricultural Science, Shanghai, 200241, PR China
[b] College of Veterinary Medicine, Xinjiang Agricultural University, Wulumuqi, 830052, Xinjiang, PR China
[c] College of Veterinary Medicine, Northwest A&F University, Yangling, 712100, Shaanxi, PR China
[d] College of Agriculture and Animal Husbandary, Qinghai University, Xining, Qinghai 810016, PR China
[e] Jiangsu Co-innovation Center for Prevention and Control of Important Animal Infectious Disease and Zoonoses, Yang Zhou, 225009, PR China

ARTICLE INFO

Keywords:
Fusion protein
Hemagglutinin-neuraminidase protein
Autophagy
Newcastle disease virus

ABSTRACT

Autophagy triggered by glycoprotein-mediated membrane fusion has been reported for several paramyxoviruses. However, the function of HN and F glycoproteins of NDV and their role in autophagy induction have not been studied. Here, we found that co-transfection of HN and F of virulent NDV rapidly induced syncytium formation and triggered a steady state autophagy flux in adenocarcinomic human alveolar basal epithelial (A549) cells and chicken embryo fibroblast (DF-1) cells. Furthermore, we clearly identified that F and HN synergistically induced autophagosome fusion with lysosomes for subsequent degradation. The seven cleavage site mutations of F significantly decreased the autophagy induction, compared with those of wildtype virulent F. RNAi and pharmacological experiments suggested that autophagy benefitted membrane fusion and syncytium formation induced by F and HN of NDV. Activated F_1 co-operated with HN to stimulate AMPK kinase and downstream ULK1 activation to suppress mTORC1 signaling. Our data described the synergistic role of HN and F in the induction of completed autophagic flux through the activation of AMPK- mTORC1- ULK1 pathway.

1. Introduction

Autophagy is a conserved catabolic process that delivers cytoplasmic contents, including foreign pathogens, such as engulfed viruses into specific double-membrane autophagosome vesicles, and shuttles to vacuoles/lysosomes for degradation and cycling (Tanida, 2011).The process of autophagic regulation is divided into several steps, namely, initiation, elongation, fusion and degradation (Paul and Munz, 2016). Autophagy types are divided into complete autophagy and incomplete autophagy based on the smooth delivery of autophagosomes into lysosome compartments for degradation (Tanida, 2011).

During the constant arms race between dead or alive, viruses manipulate different strategies to hijack autophagic machineries as a platform for their immune escape, replication, and release from infected cells for their successful survival (Paul and Munz, 2016). Most viruses interfere with two autophagy checkpoints, namely, at the early stage during autophagosome formation, and at the stage of the fusion of autophagosome with late endosomes or lysosomes (Munz, 2009). Viruses belonging to the *paramyxovirus* family like parainfluenza virus type 5 (Manuse et al., 2010), Measles virus (Joubert et al., 2009), Morbilliviruses (Delpeut et al., 2012) also utilize autophagy for progeny survival. Avian avulavirus 1, commonly known as Newcastle disease virus (NDV), belongs to the genus *Avulavirus*, family *Paramyxoviridae*, and order *Mononegavirales* (Afonso et al., 2016). NDV is generally categorized into three pathotypes based on clinical manifestations in chickens: highly virulent (velogenic), intermediate (mesogenic) or non-virulent (lentogenic) (Alexander, 2001; Czegledi et al., 2006). The genome of NDV is non-segmented, single-stranded, negative-sense with a length of about 15 kb, and encodes six proteins: nucleocapsid protein (NP), phosphoprotein (P), matrix protein (M), fusion protein (F), hemagglutinin-neuraminidase protein (HN), and polymerase protein (L) (Alexander, 2001). Two additional proteins, namely, V and W, are

* Corresponding authors at: Department of Avian Infectious Diseases, Shanghai Veterinary Research Institute, Chinese Academy of Agricultural Science, Shanghai, 200241, PR China.
E-mail addresses: sunyingjie@shvri.ac.cn (Y. Sun), shoveldeen@shvri.ac.cn (C. Ding).

https://doi.org/10.1016/j.vetmic.2019.01.002
Received 20 October 2018; Received in revised form 2 January 2019; Accepted 3 January 2019

derived from the RNA editing of the P gene (Steward et al., 1993).

Our previous studies revealed that NDV utilizes autophagy to benefit its replication in U251 glioma cells (Meng et al., 2012) and chicken embryo fibroblast (DF-1) cells (Sun et al., 2014). Another study from our lab has reported that the structural protein NP and P proteins of NDV induce autophagy via the endoplasmic reticulum stress pathway (Cheng et al., 2016). However, the molecular mechanism of autophagy induced by NDV and the role of glycoproteins remain elusive. The present study attempted to investigate the role of F and HN of NDV in the induction of autophagy and elucidate the underlying molecular mechanism.

2. Materials and methods

2.1. Cells, pharmacological reagents and antibodies

DF-1 and A549 cell lines (American Type Culture Collection, Manassas, VA, USA) were cultured in Dulbecco's modified eagle medium (DMEM) and Dulbecco's modified medium nutrient mixture F-12 (DMEM-/F-12) supplemented with 10% fetal bovine serum (FBS) (Thermo Fisher Scientific, Waltham, MA, USA), respectively. Carbonyl cyanide 3-chlorophenylhydrazone (CCCP), a drug reagent, was used as a positive control (Sigma-Aldrich, St. Louis, MO, USA). Hydroxychloroquine sulfate (HCQ) was purchased from Selleck company (S4430). Primary antibodies, including mouse anti-NP monoclonal antibody, were prepared by our laboratory (Sun et al., 2014). Anti-β-actin, anti-Flag, anti-LC3 and anti-p62/SQSTM1 were purchased from Sigma-Aldrich. Anti-ATG5, anti-HA, anti-phospho p70S6K (Thr 389), anti- p70S6K, anti-phospho 4EBP1 (Thr 37/Thr46), anti-4EBP1 and ULK1 antibody sample kit comprising phospho-AMPKα (Thr 172), AMPKα, phospho-Raptor (Ser792), Raptor, phospho-ULK1 (Ser555), phospho-ULK1 (Ser757) and ULK1were purchased from Cell Signaling Technology (Beverly, MA, USA). Secondary antibodies, including horseradish peroxidase-conjugated (HRP) goat anti-rabbit or goat anti-mouse IgG antibodies (Merck Millipore, Billerica, MA, USA) were validated for use in western blotting. Goat anti-mouse and goat anti-rabbit Alexa Fluor secondary antibodies including Alexa Fluor® 488, 594, and 633 (Molecular Probes) used for indirect immunofluorescence, were purchased from Thermo Fisher Scientific.

2.2. Plasmids

Flag-F and HA-HN plasmids were kindly gifted from Prof. Sa Xiao (Northwest A&F University, Shaanxi, China). Both viral protein plasmids were constructed on the basis of the sequence of F48E9 strain (Genbank Accession Number: MG456905), which is a standard velogenic strain. DsRed-LC3 and GFP-LC3 plasmids were prepared in our laboratory (Sun et al., 2014). The tandem technical reporter plasmid mRFP-GFP-LC3 was obtained from Prof. Tamotsu Yoshimori (Osaka University, Osaka, Japan) (Kimura et al., 2007). Seven F protein mutation plasmids were constructed by following the manufacturer's instruction of Mut Express® MultiS Fast Mutagenesis Kit V2 (Vazyme, Nanjing, China). In brief, mutation primers (Table 1) were designed to amplify the target plasmids and digested with DpnI enzyme. The amplification products were transformed into DH5α. Positive colonies were confirmed by sequencing.

2.3. Transfection and siRNA transfection

Cells were cultured at approximately 70%–80% confluence in 6-well plates and transfected with 1 μg–2 μg each of expression plasmids (GFP-LC3, ptf-LC3, DsRed-LC3, EGFP-LAMP1, Flag-F, and HA-HN) by using Lipofectamine™ 2000 Transfection Reagent (Thermo Fisher Scientific, Waltham, MA, USA) or FuGEN® HD (Promega, Madison, WI, USA) in accordance with the manufacturer's guidelines. In brief, the calculated plasmid DNA solution was mixed with a transfection reagent in an Opti-MEM reduced-serum medium for 15 min at room temperature. The mixture was added dropwise to the cells. The cells were incubated at 37 ℃ with 0.25% CO_2 for 4 h, washed twice with an Opti-MEM medium, and cultured in DMEM-/F-12 supplemented with 10% FBS for further experiments.

Three chemically synthesized siRNA oligonucleotides were obtained from Gene Pharma Company (Shanghai, China), diluted into working concentration (20 μM), and stored at −80℃ for further research. RNA interference experiment was performed in accordance with manufacturer's guidelines. In brief, A549 cells were seeded to 60% confluent in a 6-well plate. Next, an siRNA duplex with mixed with diluted Lipofectamine™ 2000 (1:1 ratio) and incubated for 15 min at room temperature. The RNA-lipid complexes were added dropwise to cells. The cells were incubated for 4 h and refreshed with 10% FBS DMEM-/F-12 for further experiments. The oligonucleotide siRNA sequences (5′ to 3′) targeting ATG5 were as follows. ATG5(#1) GACCUUUCAUUCAGA AGCUTT, ATG5(#2) GACGUUGGUAACUGACAAATT, and ATG5(#3) GUCCAUCUAAGGAUGCAAUTT.

2.4. Western blot analysis

Cell samples were washed with phosphate-buffered saline (PBS) and lysed with lysis buffer (2%SDS, 10% glycerin, 5% 2-mercaptoethanol and 0.1% bromophenol blue). The Lysates was collected into 1.5 ml tube on ice for 30 min and centrifuged at 12, 000 rpm at 4 ℃ for 15 min for clarification. The lysates were diluted into 5 × SDS buffer to a 1 × SDS final concentration. Denatured at 100 ℃ for 10 min. An equal amount of these prepared samples was subjected to sodium dodecylsulfate-polyacrylamide gel electrophoresis (SDS-PAGE) and transferred onto a nitrocellulose blotting membrane (GE Healthcare Life Science, Amersham™, Protran™ 0.2 or 0.45 NC, Germany). The membranes were then blocked with 5% skimmed milk in 0. 05% Tris-buffered saline containing 0.05% Tween 20 (TBST) for 30 min at room temperature. The membranes were washed 3 times with 0.05% TBST (5 min/each), and inoculated with primary antibodies for at least 6 h at 4 ℃. The membranes were washed thrice again with 0.05% TBST (5 min/each), and incubated with HRP-conjugated secondary antibodies at room temperature for 2 h. Lastly, after wash thrice again, the antibody-antigen complex was exposed with a chemiluminescence (ECL) reagent solution kit (Share-bio Biotechnology, Shanghai, China) by using multi-chemiluminescence image analysis system (Tanon 5200, Tanon, Guangzhou, China).

2.5. Indirect immunofluorescence assay

The A549 cells were grown on coverslips in a 6-well plate and transfected. After transfection was performed, coverslips were washed with PBS and fixed with 4% paraformaldehyde for 30 min at room temperature. Then, the cells were permeabilized with 0.5% Triton X-100 for 10 min at room temperature, washed thrice with PBS, blocked with 3% BSA at 37 ℃ for 30 min, inoculated with a primary antibody for 2 h, and washed thrice with PBS. Antibody binding was detected by using secondary antibodies conjugated with Alexa Fluor 488, 594, or 633 for 1 h in a moist container in the dark at 37 ℃. Then, the cells were stained with DAPI (0.1 μg/ml) for 8 min at 37 ℃. Finally, the coverslips were mounted on microslides and air dried. Fluorescent images were visualized and captured on a confocal fluorescence microscope (ZEISS LSM880, Germany).

3. Results and discussion

3.1. F and HN of virulent NDV induce syncytium formation in A549 cells and DF-1 cells

Autophagy triggered by viral glycoprotein has been reported for many paramyxoviruses, such as like Nipah virus, Hendra virus, Measles

Table 1
Primers used for the mutation amplification of F cleavage site in this study.

Primer Name	Primer sequence (5' - 3')
F^{112} Forward	TCCGGAGGA***G***GGAGGCAGAGACGCTTTATAGGTGCCATTATC
F^{112} Reverse	TGCCTCC***C***TCCTCCGGACGTAGTC GCAGACTCTTGTATCC
F^{115} Forward	AGGCAG***G******G***CGCTTTATAGGTGCCATTATCGGCAGTGTAGCTC
F^{115} Reverse	ATAAAGCG***C******C***CTGCCTCCTTCCTCCGGACGTAGTCGCAGACTCTTG
F^{117} Forward	AGAGACGC***C***TTATAGGTGCCATTATC GGCAGTGTAGCTCTTGGGG
F^{117} Reverse	GCACCTATAA***G***GCGTCTCTGCCTCCTTCCTCCGGACGTAGTC
$F^{112+115}$ Forward	AGGA***G***GGAGGCAG***G******G***CGCTTTATAGGTGCCATTATCGGCAGTGTAGC
$F^{112+115}$ Reverse	AAGCG***C******C***CTGCCTCC***C***TCCTCCGGACGTAGTCGCAGACTCTTGTATC
$F^{112+117}$ Forward	AGGA***G***GGAGGCAGAGACGC***C***TTATAGGTGCCATTATCGGCAGTGTAGC
$F^{112+117}$ Reverse	ATAA***G***GCGTCTCTGCCTCC***C***TCCTCCGGACGTAGTCGCAGACTCTTG
$F^{115+117}$ Forward	AGGAAGGAGGCAG***G******G***CGC***C***TTATAGGTGCCATTATCGGCAGTGTAGCTC
$F^{115+117}$ Reverse	CTATAA***G***GCG***C******C******C***TGCCTCCTTCCTCCGGACGTAGT CGCAGACTCTTGTATCC
$F^{112+115+117}$Forward	AGGA***G***GGAGGCAG***G******G***CGC***C***TTATAGGTGCCATTATCGGCAGTGTAGCTCTTGGGGTTG
$F^{112+115+117}$ Reverse	CCTATAA***G***GCG***C******C******C***TGCCTCC***C***TCCTCCGGACGTAGTCGCAGACTCTTGTATCCTGCGG

The F sequence above was referred to as F48E9 (Genbank Accession Number: MG456905), which is a standard velogenic strain. In this study, the velogenic NDV (F48E9) F amino acids R, R, and F were mutated into the lentogenic NDV (La Sota) F amino acids G, G, and L through a single mutation at 112, 115, and117, through double mutations at 112/115, 112/117, and 115/117, and through triple mutations at 112/115/117, respectively. The velogenic F nucleotides at 112 A, 115 A and 117 T were mutated into the lentogenic F nucleotides G, G,and C, respectively. The mutated nucleotides were marked in bold red italics above.

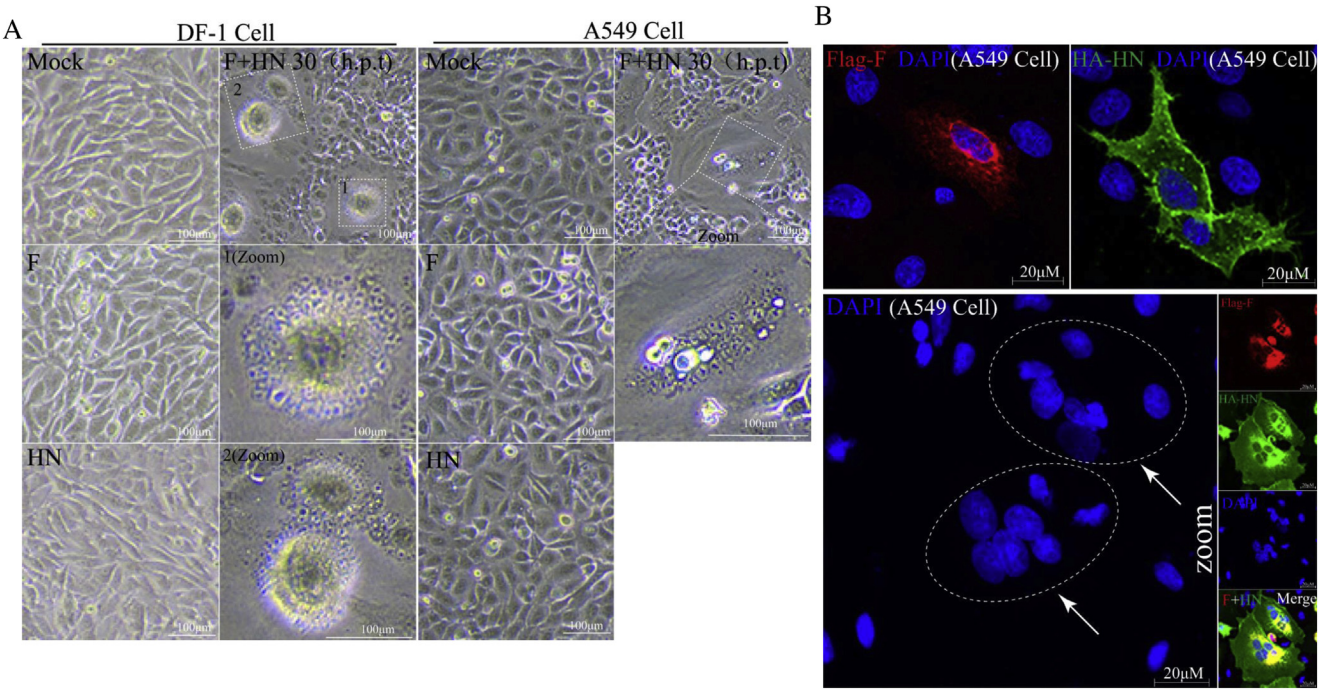

Fig. 1. F and HN of virulent NDV induce syncytium formation in A549 cells and DF-1 cells.
(A) Observation of syncytium formation in DF-1 cells and A549 Cells. DF-1 cells and A549 Cells were transfected with plasmids Flag-F, HA-HN, or both. After 30 h post-transfection (h.p.t), gray images were visualized and captured using a microscope. Syncytium formation could be observed on the basis of nuclei and indicated by a white quadrangle.
(B) IFA assay of Syncytium formation in A549 cells. At18 h.p.t, fluorescent images were visualized and captured using a confocal fluorescence microscope. Syncytia were observed on the basis of nuclei and indicated by a white dot circle.

viruses, and Mumps virus (Delpeut et al., 2012). NDV infects cells by initially attaching to a sialic-containing cellular receptor via HN protein and subsequently fusing with the plasma membrane by interacting with F protein (Chang and Dutch, 2012; Smith et al., 2009). However, studies have yet not to elucidate the involvement of F and HN glycoproteins in NDV induced autophagy and the underlying mechanism. As such, we co-transfected F and HN plasmids in DF-1 and A549 cells. As expected, the significant syncytium formation was observed in HN and F co-transfected DF-1 cells (Fig. 1A). HN and F co-transfection also triggered obvious syncytia in A549 cells (Fig. 1A and B). Those data suggested that F cooperating with HN induced an efficient membrane fusion in DF-1 and A549 cells. The number of syncytia formed in DF-1 and A549 cells increased in a time- and dose-dependent manner (Data not shown). Taken together, all these data suggested the virulent F and HN triggered syncytium formation in A549 cells and DF-1 cells, suggesting that they could be used as a cell model to study the function of both glycoproteins.

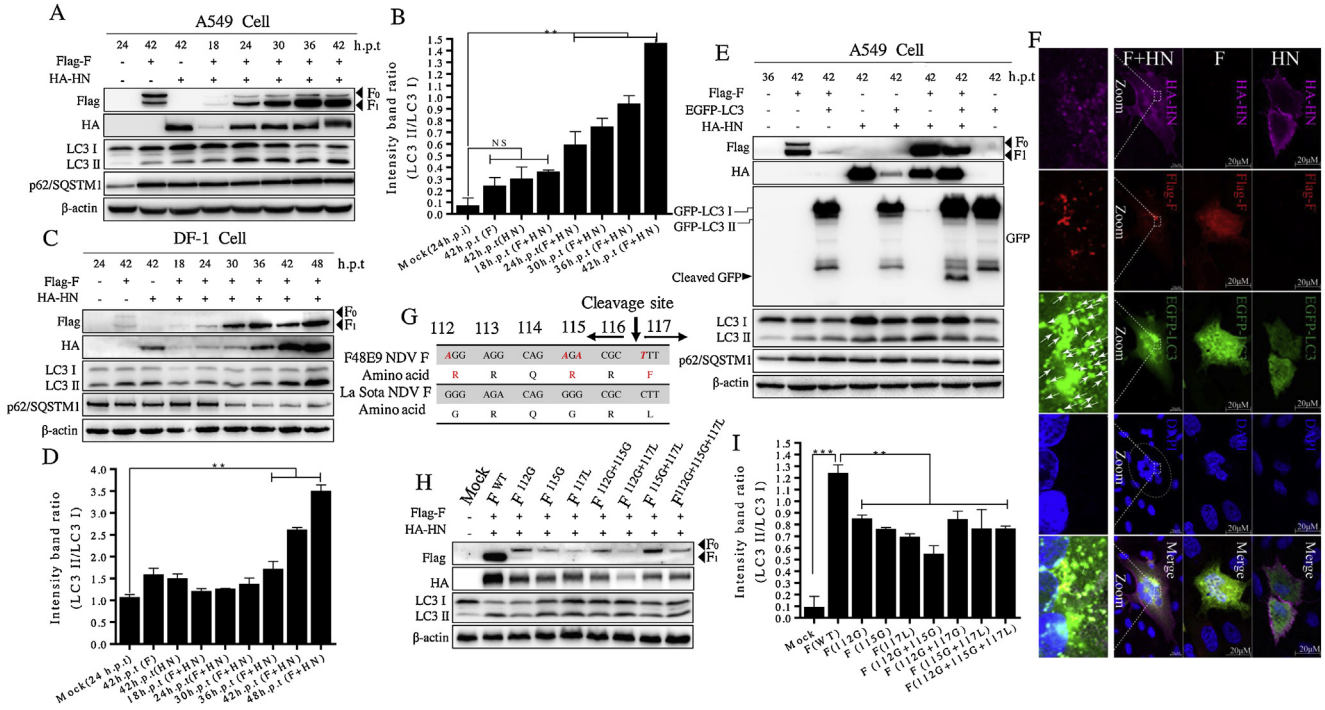

Fig. 2. F and HN cooperate synergistically to induce autophagic flux in A549 cells and DF-1 cells.

(A) LC3-I conversion and LC3-II turnover assay in A549 cells.

(B) Intensity band ratio of LC3 II to LC3 I. Data were presented as means from three independent statistical experiments. The intensities of protein bands were quantified using Image J (National Institutes of Health, Bethesda, MD, USA). Significance was analyzed using a one-tailed Student's t-test. NS, no significance; **, *p*-value < 0.01.

(C) LC3-I conversion and LC3-II turnover assay in DF-1cells.

(D) Intensity band ratio of LC3 II to LC3 I. Data were presented as means from three independent statistical experiments. The intensities of protein bands were quantified using Image J.

(E) GFP-LC3 cleavage turnover assay. Western-blot samples corresponding to the marked time-points were collected and analyzed in accordance with procedures in the Materials and Methods.

(F) Accumulation of the punctum formation of EGFP-LC3 positive punctum assay. A549 cells were transfected with F, HN, and both. At 24 h.p.t, fluorescent images were visualized and captured using a confocal fluorescence microscope. The representative LC3 puncta were indicated with a white arrow.

(G) Sequence of targeted mutation sites for the synthesis of F protein cleavage site mutation plasmid. F sequence was referred to as F48E9 (Genbank Accession Number: MG456905), which is a standard velogenic strain, and La Sota (Genbank Accession Number: JF950510.1), which is a standard lentogenic strain. In this study, the velogenic F nucleotides (upper panel) at 112 A, 115 A, and 117 T were mutated into the lentogenic F nucleotides G, G, and C (lower panel), respectively, which were marked in red italics. Eventually, the velogenic NDV F amino acids R, R and F (upper panel) were mutated into the lentogenic NDV F amino acids G, G, and L (lower panel) through single mutations at 112, 115, and 117, through double mutations at 112/115, 112/117, and 115/117, and through triple mutations at 112/115/117, respectively.

(H) Cleavage site motif of F influences the autophagy induction. In A549 cells, wild type HN plasmid was co-transfected with wild-type F, F^{112G}, F^{115G}, F^{117L}, $F^{112G+115G}$, $F^{112G+117L}$, $F^{115G+117L}$ and $F^{112G+115G+117L}$, respectively. Western-blot samples corresponding to the marked time-points were collected and analyzed in accordance with procedures in the Materials and Methods.

(I) Intensity band ratio of LC3 II to LC3 I. Data were presented as means from three independent statistical experiments. The intensities of protein bands were quantified using Image J (National Institutes of Health, Bethesda, MD, USA). Significance was analyzed using a one-tailed Student's t-test. *, *p*-value < 0.05; **, *p*-value < 0.01; ***, *p*-value < 0.001.

3.2. F and HN cooperate synergistically to induce autophagic flux in A549 cells and DF-1 cells

Autophagic flux was monitored using several methods, such as microtubule-associated protein light chain 3 (LC3)-II turnover assays, GFP-LC3 processing assay, and examination of the punctum formation of green fluorescent protein (GFP)-LC3 (Klionsky et al., 2016). In general, the LC3 II turnover assay is used as classical method to investigate the autophagic flux dynamics (Tanida et al., 2005). To investigate whether F and HN induced autophagy in A549 cells or DF-1 cells, we co-transfected both glycoproteins in A549 and DF-1 cells (Fig. 2A and C). As shown in Fig. 2B and D, western blot analyses revealed that co-transfection of F and HN in both cell types leads to increased ratio of LC3-II to LC3-I in a time-dependent manner. Previous studies reported that p62/SQSTM1 protein was incorporated into a complete autophagosome and degraded in autolysosomes by linking an autophagic machinery and ubiquitinated substrates via the LC3-interacting region (LIR) and a ubiquitin binding domain (UBA) (Bjorkoy et al., 2005). As such, the p62/SQSTM1 turnover assay was also performed to determine the autophagy flux activity. As expected, p62/SQSTM1 protein degraded in time-dependent manner in DF-1 cells, suggesting the smooth activation of the autophagy flux (Fig. 2C). However, surprisingly, the degradation of p62/SQSTM1 was not observed in the co-transfected A549 cells (Fig. 2A). Here, we speculated that the difference in the results of p62/SQSTM1 level in A549 and DF-1 cells mainly because of the difference in cell lines, because the degradation of the p62/SQSTM1 was specific to cell type and context (Klionsky et al., 2016). In some cell types, p62/SQSTM1 remains unchanged despite strong autophagy flux (Klionsky et al., 2016). The robust loss of p62/SQSTM1 was even related to a blockage of autophagy, because of the cleavage by other autophagic proteins, such as caspases or calpains (El-Khoury et al., 2014). For example, in acute myeloid leukemia cells, an increase autophagic flux is induced by all-*trans*-retinoic acid concomitant with increased p62/SQSTM1 levels (Trocoli et al., 2014, 2011). These

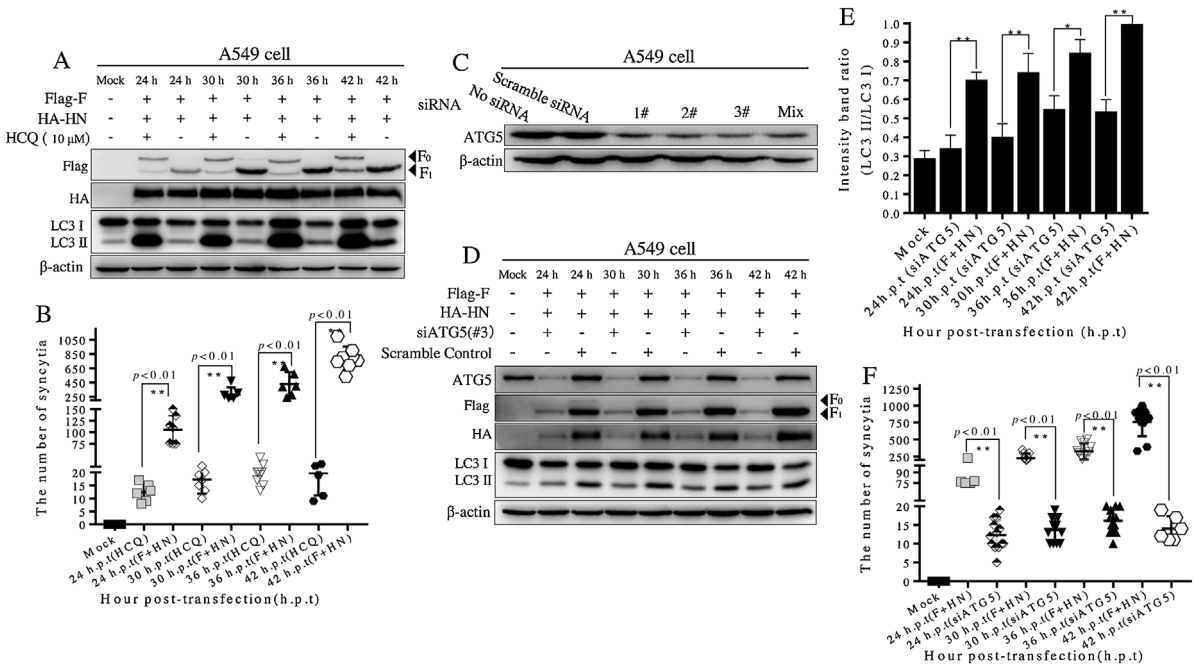

Fig. 3. Complete autophagic flux benefits syncytium formation induced by F and HN.

(A) Western blot results of autophagic flux inhibited by CQ. A549 cells were initially pretreated with CQ (10 μM) for 2 h before transfection and subsequently co-transfected with Flag-F and HA-HN plasmids in the absence or presence of CQ. At different time points, lysates were collected and analyzed through immunoblot analysis with indicated antibodies. WST-1 assay showed that the viability of A549 cells was not significantly affected by CQ treated at 10 μM (data not shown).

(B) Observation of syncytium formation in A549 cells. A549 cells were co-transfected with both Flag-F and HA-HN plasmids in the absence or presence of CQ. Syncytium formation could be observed on the basis of the number of nuclei. Numerical data were the average number of syncytia in different microscope fields in at least three independent experiments. Significance was analyzed using a one-tailed Student's t-test. *, p-value < 0.05; **, p-value < 0.01.

(C) Detection of the inhibition efficiency of ATG5 by ATG5-specific siRNAs.

(D) Detection of ATG5 siRNA through Western blot analysis.

A549 cells were transfected with scrambled siRNA or ATG5 siRNA (#3) for 24 h.p.t, and co-transfected with Flag-F and HA-HN. At different time points, the lysates were collected and analyzed through immunoblot analysis with the indicated antibodies. Scramble siRNA was used as a negative control.

(E) Intensity band ratio of LC3 II to LC3 I. Data were presented as means from three independent statistical experiments. The intensities of protein bands were quantified using Image J. Significance was analyzed using a one-tailed Student's t-test. *, p-value < 0.05; **, p-value < 0.01.

(F) Observation of syncytium formation in A549 cells. A549 cells were transfected with scrambled siRNA or ATG5 siRNA (#3) for 24 h.p.t and co-transfected with F and HN. Syncytium formation could be observed on the basis of the nuclei number. Numerical data were the average number of syncytia at different microscope fields in at least three independent experiments. Significance was analyzed using a one-tailed Student's t-test. *, p-value < 0.05; **, p-value < 0.01.

findings suggested that p62/SQSTM1 degradation was not always positively correlated with autophagic flux. The transfected GFP-LC3 was delivered to a lysosome or a vacuole, and the LC3 part of the chimera was easily degraded. Conversely, the free GFP was relatively resistant to hydrolysis (Klionsky et al., 2016). Thus, the detection of free GFP by using western blot could be used to monitor the lysis of inner autophagosome membrane. In this study, we examined the cleaved free GFP in the co-transfected A549 cells. In Fig. 2E, the cleaved GFP in the co-transfected A549 cells demonstrated the lysosomal delivery and partial proteolysis of GFP-LC3. An increased number of the GFP-positive puncta was found in the co-transfected A549 cells by using a GFP-tagged LC3 plasmid (Fig. 2F), indicating autophagosome accumulation. In general, virulent NDV strains contain a multi-basic amino acid-rich region (^{112}R/K-R-X-R/K-R-F^{117}) in the cleavage site, whereas avirulent strains possess a ^{112}G/E-K/R-X-G/E-R-L^{117} motif cleaved by the secreted trypsin-like protease into an active F protein, which consists of disulphide-linked F_1 and F_2 polypeptides (Glickman et al., 1988; Nagai et al., 1976; Smith et al., 2009). Seven F cleavage site mutative plasmids were prepared (Fig. 2G) to examine the role of the cleavage site motif of F protein, along with HN on autophagy induction. As show in Fig.2H, those seven site mutations significantly affected the autophagy induction compared with the wild type F protein, as indicated by the ratio of LC3-II to LC3-I (Fig.2 I). Therefore, the cleavage ability of F protein precursor (F_0) was essential for F and HN synergistic autophagy induction.

3.3. Autophagy benefits syncytium formation induced by F and HN

To analyze the effect of complete autophagy on syncytium formation induce by F and HN of virulent NDV, we examined pharmacological inhibition. Hydroxychloroquine Sulfate (HCQ) is a potent inhibitor of autophagy at the late stage, thereby preventing lysosomal acidification and causing the accumulation of sequestered materials. In this study, comparison with the F and HN co-transfection group, the HCQ treatment group significantly decreased the fusogenically active F_1 expression (Fig. 3A), indicating that autophagy facilitated the cleavage of F_0 into F_1. HCQ drug treatment significantly decreased the number of syncytia induced by both glycoproteins (Fig. 3B), suggesting that the pharmacological inhibition of autophagy significantly reduced syncytium formation ability. Meanwhile, to avid the pharmacological non-specific effect on the cell, we next experimentally studied the knockdown of autophagy-related genes (ATGs) with small interfering RNAs(siRNAs). Autophagy related 5 (ATG5) is a key protein involved in the extension of the phagophoric membrane in autophagic vesicles, which is necessary for LC3 I conjugation to phosphatidylethanolamine to form LC3 II (Klionsky et al., 2016). In Fig. 3 C, ATG5 siRNAs (#3) exhibited an obvious inhibition efficiency of endogenous ATG5. In comparison with F and HN positive group, the siATG5(#3) group significantly decreased the ratio of LC3I/LC3II (Fig. 3D and E), suggesting that F could not smoothly cooperate with HN to synergistically induce autophagic flux in A549 cells. We also found the knockdown of

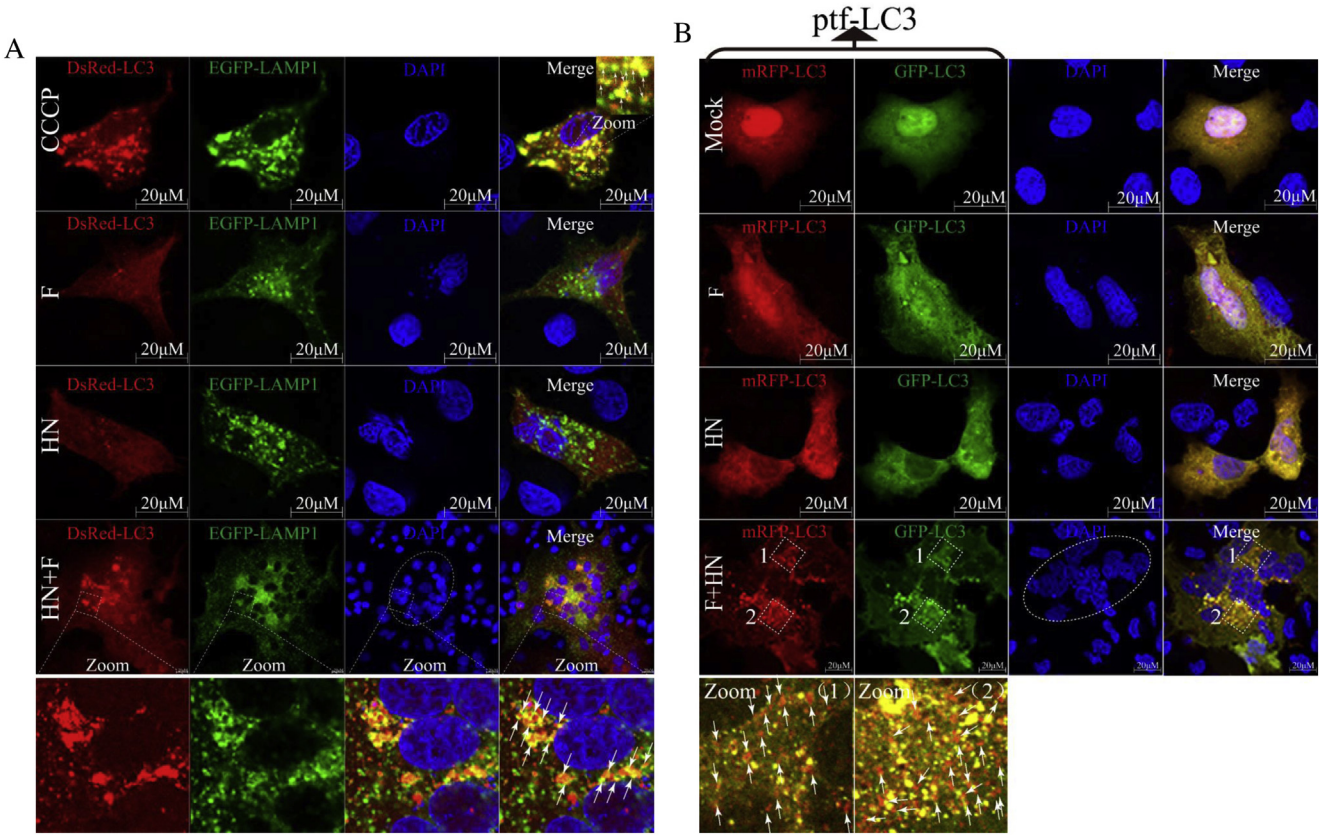

Fig. 4. F with HN cooperates synergistically to induce complete autophagic flux in A549 cells.
(A) Detection of the colocalization between autophagic flux and lysosomes. DsRed-LC3 and EGFP-LAMP1 plasmids were co-transfected into A549 cells with plasmid Flag-F, HA-HN or both for 24 h. After transfection was performed, fluorescent images were visualized and captured using a confocal fluorescence microscope. The representative co-localization dots among LC3 and LAMP1 were indicated by yellow puncta. White arrows point to typical examples of the colocalized particles of LC3 and LAMP1 signals.
(B) Detection of GFP and mRFP signals of tandem fluorescent LC3. The ptf-LC3 plasmid was co-transfected into A549 cells with Flag-F, HA-HN or both. At 24 h.p.t, fluorescent images were visualized and captured using a confocal fluorescence microscope. These typical examples of red fluorescence signals were marked with white arrows.

endogenous ATG5 significantly reduced F and HN proteins compared with that of the positive control, indicating that an autophagic machinery was required for the effective interaction between F and HN complex (Fig. 3D). The knockdown of endogenous ATG5 significantly decreased the number of syncytia as induced by F and HN (Fig. 3F), suggesting that autophagy benefitted syncytium formation. Therefore, RNAi and pharmacological experiments indicated that autophagy contributed to membrane fusion and syncytium formation induced by F and HN of NDV.

3.4. F with HN cooperates synergistically to induce a complete autophagic flux in A549 cells

Considering that exogenous GFP-LC3 punctum accumulation and increase in endogenous LC3 II might be the result of an increased formation or a decreased degradation of autophagosomes. We assessed the colocalization between autophagosomes and lysosomes, marked with the targeted plasmids DsRed-LC3 and EGFP-LAMP1, respectively. Lysosomal-associated membrane protein 1 (LAMP1) is the late endosome and lysosome marker that localizes with LC3 during autolysosome maturation. Confocal microscopy imaging revealed the co-colocalization of DsRed-LC3 and EGFP-LAMP1 in co-transfected and CCCP reagent-treated A549 cells (Fig.4A), indicating the smooth fusion of the autophagosomes with lysosomes. To confirm these results, we assessed the fluorescent changes by using a tandem both green fluorescent protein (GFP) and red fluorescent protein (RFP) reporter technical plasmid, named ptf-LC3 (Kimura et al., 2007). GFP quickly quenches the fluorescence in a lysosomal environment with acidic pH and undergoes proteolysis, whereas RFP retains fluorescence in an acidic pH environment (Klionsky et al., 2016). Increased RFPs were observed in the co-transfected A549 cells (Fig.4B) marked with a white arrow, compared with those in the single transfected and mock-A549 cells, suggesting that an autophagic flux fuses with lysosomes for subsequent degradation. In summary, those data demonstrated F and HN synergistically triggered complete autophagy.

3.5. F cooperates with HN and synergistically activates AMPK-ULK1-mTORC1 signaling in A549 cells

The main autophagic signal pathway was determined to clarify the molecular mechanism of complete autophagy induced by F and HN. From a system point of view, autophagy is the result of imbalance in key metabolic sensors. Adenosine monophosphate-activated protein kinase (AMPK) is an enzyme that acts as a fine-tuned sensor of the overall cellular energy status and maintains energy homeostasis (Carling et al., 2011). The enzymatic activity of AMPK depends on the phosphorylation of the AMPK1α subunit on Thr172 (Hawley et al., 1996). An increased expression of the phosphorylation of AMPK at Thr172 (Fig. 4A) indicated the activation of AMPK enzymatic activity. The mammalian target of rapamycin complex 1 (mTORC1), another major sensor of the energy state, is composed of mTORC1, Raptor, PRAS40, mLST8, and DEPTOR (Inoki et al., 2002). In mammalian cells,

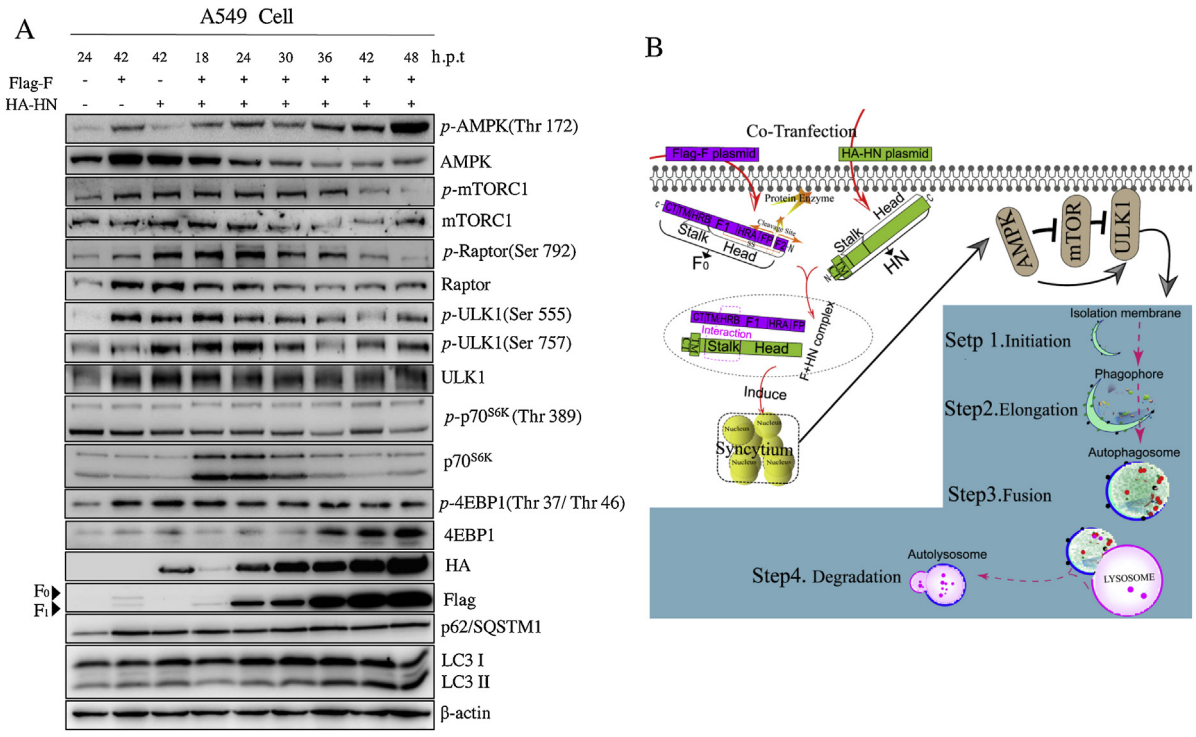

Fig. 5. F cooperating with HN synergistically activates an AMPK-ULK1-mTORC1 signaling in A549 cells.
(A) Western blot analysis. Western-blot samples corresponding to the marked time-point were collected and performed.
(B) Model pattern of the activation of AMPK-ULK-mTORC1 signaling pathway to initiate complete autophagy by the co-transfection of virulent F and HN plasmids. After transfection was conducted, the no-fusogenic F protein precursor (F_0) form should be proteolytically cleaved into a disulfide-linked F1 + F2 heterodimer, to be fusogenically active. This step is an essential for fusion by positioning FP at the newly formed N-terminus of F1(Chang and Dutch, 2012; Smith et al., 2009). Then, the fusogenically active F protein and HN form an F + HN complex via the interaction between a stalk and an HRB domain (Gravel and Morrison, 2003; Melanson and Iorio, 2006). Once triggered, HRB complete refolds around HRA, thereby forming stable 6 HB and a fusion pore (Chang and Dutch, 2012), and consequently inducing membrane fusion and syncytium formation. Eventually, fusogenically active F cooperates with HN to synergistically activate AMPK-ULK1-mTORC1 signaling and initiate autophagic flux and subsequent degradation(Kim et al., 2010).
For all images, the following domain abbreviations were used: hydrophobic fusion peptide (FP), two heptad repeat regions (HRA + HRB), a single-pass transmembrane domain (TM), a c-terminal cytoplasmic tail (CT) domain, a stalk domain(Stalk), and head domain(Head) (Smith et al., 2009).

in response to growth factors, mTORC1 directly phosphorylates the eukaryotic translation initiation factor 4E binding protein (4EBP1, also known as EIF4EBP1) at Thr 37 and Thr 46 and ribosomal protein S6 kinase ($p70^{S6k}$, also known as RPS6K) at Thr389 to promote protein synthesis (Shimobayashi and Hall, 2014; Yip et al., 2010). Under nutrient-rich conditions, mTORC1 phosphorylates unc-51 like autophagy activating kinase 1(ULK1), a kinase specifically involved in early steps of autophagosome, to inhibit its interaction with AMPK, leading to the suppression of autophagy (Kim et al., 2011). On the contrary, cellular energy depletion induces AMPK-mediated mTORC1 inhibition and then leads to autophagy induction (Klionsky et al., 2016). We also monitored mTORC1 activity by directly assessing the phosphorylation state of mTORC1, 4EBP1, p70S6k, and Raptor. We found that F and HN decreased the phosphorylation level of mTORC1, regulator Raptor and downstream protein 4EBP1 and $p70^{S6k}$, especially $p70^{S6k}$ (Fig. 5A), suggesting the functional inhibitory effect of mTORC1. AMPK and mTORC1 regulate autophagy through the coordinated phosphorylation of ULK1 (Klionsky et al., 2016). Under sufficient nutrient conditions, a high mTORC1 activity suppresses ULK1 activation by disrupting the interaction between ULK1 and AMPK and by phosphorylating ULK1 residues. The phosphorylation of ULK1 at Ser 555 is indicative of an increased autophagy in response to nutrient stress, in which Ser 757 is targeted by mTOR to inhibit autophagy (Klionsky et al., 2016). The co-expression of F and HN directly regulates the phosphorylation state of ULK at Ser 555 and at Ser 757 to ultimately initiate autophagy by evading mTOR inhibition (Fig. 5A). In summary, the activated F1 protein cooperated with HN to synergistically activate AMPK-mTOR-ULK1 signaling for the initiation of a complete autophagic flux and the subsequent degradation in lysosomes (Fig.5B).

4. Conclusion

HN and F of virulent NDV significantly induce syncytium formation and trigger a steady state autophagy flux in A549 cells and DF-1 cells, which smoothly fuse with lysosomes for subsequent degradation. The cleavage site of F significantly affects autophagy induction. RNAi and pharmacological experimental data suggest that autophagy benefits membrane fusion and syncytium formation induced by F and HN of NDV. After F_0 is cleaved into F_1 and F_2, fusogenically active F_1 cooperates with HN to stimulate AMPK kinase and downstream ULK1 activation to suppress mTORC1 activity. Our results describe the synergistic role of HN and F of NDV in the induction of complete autophagic flux and subsequent degradation through the activation of AMPK-mediated mTORC1, and ULK1 pathway.

Conflict of interest statement

All listed authors declare no competing financial interest.

Acknowledgements

This work was funded by the National Key Research and Development Program of China (No.2018YFD0500100) and National Natural Science Foundation of China (No.31530074, 31872453). We thank Dr. Chongyang Wang and Na Huo (Northwest A& F University) for technical support and for Dr. Yanqing Jia (Northwest A& F

University) for moral encouragement.

References

Afonso, C.L., Amarasinghe, G.K., Banyai, K., Bao, Y., Basler, C.F., Bavari, S., et al., 2016. Taxonomy of the order Mononegavirales: update 2016. Arch. Virol. 161, 2351–2360.

Alexander, D.J., 2001. Gordon memorial lecture. Newcastle disease. Br. Poult. Sci. 42, 5–22.

Bjorkoy, G., Lamark, T., Brech, A., Outzen, H., Perander, M., Overvatn, A., Stenmark, H., Johansen, T., 2005. p62/SQSTM1 forms protein aggregates degraded by autophagy and has a protective effect on huntingtin-induced cell death. J. Cell Biol. 171, 603–614.

Carling, D., Mayer, F.V., Sanders, M.J., Gamblin, S.J., 2011. AMP-activated protein kinase: nature's energy sensor. Nat. Chem. Biol. 7, 512–518.

Chang, A., Dutch, R.E., 2012. Paramyxovirus fusion and entry: multiple paths to a common end. Viruses 4, 613–636.

Cheng, J.H., Sun, Y.J., Zhang, F.Q., Zhang, X.R., Qiu, X.S., Yu, L.P., Wu, Y.T., Ding, C., 2016. Newcastle disease virus NP and P proteins induce autophagy via the endoplasmic reticulum stress-related unfolded protein response. Sci. Rep. 6, 24721.

Czegledi, A., Ujvari, D., Somogyi, E., Wehmann, E., Werner, O., Lomniczi, B., 2006. Third genome size category of avian paramyxovirus serotype 1 (Newcastle disease virus) and evolutionary implications. Virus Res. 120, 36–48.

Delpeut, S., Rudd, P.A., Labonte, P., von Messling, V., 2012. Membrane fusion-mediated autophagy induction enhances morbillivirus cell-to-cell spread. J. Virol. 86, 8527–8535.

El-Khoury, V., Pierson, S., Szwarcbart, E., Brons, N.H., Roland, O., Cherrier-De Wilde, S., Plawny, L., Van Dyck, E., Berchem, G., 2014. Disruption of autophagy by the histone deacetylase inhibitor MGCD0103 and its therapeutic implication in B-cell chronic lymphocytic leukemia. Leukemia 28, 1636–1646.

Glickman, R.L., Syddall, R.J., Iorio, R.M., Sheehan, J.P., Bratt, M.A., 1988. Quantitative basic residue requirements in the cleavage-activation site of the fusion glycoprotein as a determinant of virulence for Newcastle disease virus. J. Virol. 62, 354–356.

Gravel, K.A., Morrison, T.G., 2003. Interacting domains of the HN and F proteins of newcastle disease virus. J. Virol. 77, 11040–11049.

Hawley, S.A., Davison, M., Woods, A., Davies, S.P., Beri, R.K., Carling, D., Hardie, D.G., 1996. Characterization of the AMP-activated protein kinase kinase from rat liver and identification of threonine 172 as the major site at which it phosphorylates AMP-activated protein kinase. J. Biol. Chem. 271, 27879–27887.

Inoki, K., Li, Y., Zhu, T., Wu, J., Guan, K.L., 2002. TSC2 is phosphorylated and inhibited by Akt and suppresses mTOR signalling. Nat. Cell Biol. 4, 648–657.

Joubert, P.E., Meiffren, G., Gregoire, I.P., Pontini, G., Richetta, C., Flacher, M., Azocar, O., Vidalain, P.O., Vidal, M., Lotteau, V., Codogno, P., Rabourdin-Combe, C., Faure, M., 2009. Autophagy induction by the pathogen receptor CD46. Cell Host Microbe 6, 354–366.

Kim, H.J., Lee, S., Jung, J.U., 2010. When autophagy meets viruses: a double-edged sword with functions in defense and offense. Semin. Immunopathol. 32, 323–341.

Kim, J., Kundu, M., Viollet, B., Guan, K.L., 2011. AMPK and mTOR regulate autophagy through direct phosphorylation of Ulk1. Nat. Cell Biol. 13, 132–141.

Kimura, S., Noda, T., Yoshimori, T., 2007. Dissection of the autophagosome maturation process by a novel reporter protein, tandem fluorescent-tagged LC3. Autophagy 3, 452–460.

Klionsky, D.J., Abdelmohsen, K., Abe, A., Abedin, M.J., Abeliovich, H., et al., 2016. Guidelines for the use and interpretation of assays for monitoring autophagy (3rd edition). Autophagy 12, 1–222.

Manuse, M.J., Briggs, C.M., Parks, G.D., 2010. Replication-independent activation of human plasmacytoid dendritic cells by the paramyxovirus SV5 requires TLR7 and autophagy pathways. Virology 405, 383–389.

Melanson, V.R., Iorio, R.M., 2006. Addition of N-glycans in the stalk of the Newcastle disease virus HN protein blocks its interaction with the F protein and prevents fusion. J. Virol. 80, 623–633.

Meng, C., Zhou, Z., Jiang, K., Yu, S., Jia, L., Wu, Y., Liu, Y., Meng, S., Ding, C., 2012. Newcastle disease virus triggers autophagy in U251 glioma cells to enhance virus replication. Arch. Virol. 157, 1011–1018.

Munz, C., 2009. Enhancing immunity through autophagy. Annu. Rev. Immunol. 27, 423–449.

Nagai, Y., Klenk, H.D., Rott, R., 1976. Proteolytic cleavage of the viral glycoproteins and its significance for the virulence of Newcastle disease virus. Virology 72, 494–508.

Paul, P., Munz, C., 2016. Autophagy and mammalian viruses: roles in immune response, viral replication, and beyond. Adv. Virus Res. 95, 149–195.

Shimobayashi, M., Hall, M.N., 2014. Making new contacts: the mTOR network in metabolism and signalling crosstalk. Nat. Rev. Mol. Cell Biol. 15, 155–162.

Smith, E.C., Popa, A., Chang, A., Masante, C., Dutch, R.E., 2009. Viral entry mechanisms: the increasing diversity of paramyxovirus entry. FEBS J. 276, 7217–7227.

Steward, M., Vipond, I.B., Millar, N.S., Emmerson, P.T., 1993. RNA editing in Newcastle disease virus. J. Gen. Virol. 74 (Pt 12), 2539–2547.

Sun, Y., Yu, S., Ding, N., Meng, C., Meng, S., Zhang, S., Zhan, Y., Qiu, X., Tan, L., Chen, H., Song, C., Ding, C., 2014. Autophagy benefits the replication of Newcastle disease virus in chicken cells and tissues. J. Virol. 88, 525–537.

Tanida, I., 2011. Autophagosome formation and molecular mechanism of autophagy. Antioxid. Redox Signal. 14, 2201–2214.

Tanida, I., Minematsu-Ikeguchi, N., Kominoma, T.U.K., Ea, C.K., 2005. Lysosomal Turnover but Not a Cellular Level of Endogenous LC3 is a Marker for Autophagy. Autophagy 1, 2.

Trocoli, A., Mathieu, J., Priault, M., Reiffers, J., Souquere, S., Pierron, G., Besancon, F., Djavaheri-Mergny, M., 2011. ATRA-induced upregulation of Beclin 1 prolongs the life span of differentiated acute promyelocytic leukemia cells. Autophagy 7, 1108–1114.

Trocoli, A., Bensadoun, P., Richard, E., Labrunie, G., Merhi, F., Schlafli, A.M., Brigger, D., Souquere, S., Pierron, G., Pasquet, J.M., Soubeyran, P., Reiffers, J., Segal-Bendirdjian, E., Tschan, M.P., Djavaheri-Mergny, M., 2014. p62/SQSTM1 upregulation constitutes a survival mechanism that occurs during granulocytic differentiation of acute myeloid leukemia cells. Cell Death Differ. 21, 1852–1861.

Yip, C.K., Murata, K., Walz, T., Sabatini, D.M., Kang, S.A., 2010. Structure of the human mTOR complex I and its implications for rapamycin inhibition. Mol. Cell 38, 768–774.